Supplementary Information

Novel Cobalt/Nickel-Tungsten-Sulfide Catalysts for Electrocatalytic Hydrogen Generation from Water

Phong D. Tran,[*a,b] Sing Yang Chiam,[c] Pablo P. Boix,[a] Yi Ren,[c] Stevin S. Pramana,[d] Jennifer Fize,[e] Vincent Artero,*[e] James Barber[*b,f,g]

[a]*Energy Research Institute @ NTU, Nanyang Technological University, Singapore; Email: dptran@ntu.edu.sg*

[b]*Solar Fuel Laboratory, School of Materials Science and Engineering, Nanyang Technological University, Singapore.*

[c]*Institute of Materials Research and Engineering, ASTAR, Singapore*

[d]*Facility of Analysis, Characterization, Testing and Simulation (FACTS), Nanyang Technological University, Singapore*

[e]*Laboratoire de Chimie et Biologie des Métaux, Université Grenoble 1/CNRS/CEA, Grenoble, France; Email: Vincent.artero@cea.fr*

[f]*Department of Life Sciences, Imperial College London, London SW7 2AZ, UK; Email: j.barber@imperial.ac.uk*

[g]*Applied Science and Technology Department–BioSolar Lab, Politecnico di Torino, Italy*

1. Materials and Methods

All chemical compounds were in analytical grade and used as received without further purification. Fluorine-doped tin oxide (FTO) coated glass slides with 14 Ω/sq resistivity and a thickness of 400 nm were purchased from NSG group. FTO electrode was cleaned by subsequent sonication in acetone, isopropanol and ethanol and then dried by a nitrogen gas flux before used.

Electrochemical experiments were performed on an Autolab PGSTAT-30 or a Bio-Logic SP 300 potentiostat employing a conventional three electrodes configuration. Customized two compartment electrochemical cell was used. The working electrode was the synthesized catalyst film on 1cm^2 FTO or 0.071 cm^2 carbon glassy electrode. Reference electrode was an Ag/AgCl 3M KCl, purchased from CH Instruments, while counter electrode was a Pt mesh. Reference electrode was calibrated daily by employing a solution of $[Fe(CN)_6]^{3-}/[Fe(CN)_6]^{4-}$ in pH 7 potassium phosphate buffer.

Potentials are reported versus the Ag/AgCl reference employed. To determine overpotential value, potential are quoted against the *Reversible Hydrogen Electrode* (RHE) by using the following equation:

$$E_{vs.\ RHE} = E_{vs.\ Ag/AgCl} + 0.059pH + 0.21V$$

Cyclic voltammograms (50mV.s^{-1}) and linear sweep voltammograms (2mV.s^{-1}) were recorded in 0.1M phosphate solutions buffered at various pHs. Prior to measurement, phosphate solutions were saturated with research grade hydrogen gas in order to maintain the potential of the $2H^+/H_2$ redox couple during the potential polarization on MWS_x electrode.

Potential polarization experiments coupled with H_2 quantification were carried out in a home-made gas-tight closed electrochemical cell. A conventional three electrodes configuration was adopted. The working electrode was the MWS_x/FTO (1cm^2) while the

reference electrode was an Ag/AgCl, 3M KCl and the auxiliary electrode was a Pt wire. Potential polarization was done at very slow potential rate of $0.05mV.s^{-1}$. The gas produced in the cell was directly sampled and analysed by gas chromatography using the same setup as previously described [*ref. 1*]. This allowed the determination of the actual practical on-set potential where hydrogen production is detectable.

The same gas-tight closed electrochemical cell and setup was employed for bulk electrolysis experiment and GC analysis in the "continuous flow" mode allowing the determination of the faradic yield for H_2 evolution. The deviation between theoretical and experimentally quantified H_2 amount is likely due to the adherence of H_2 bubbles on the electrode and glassware surface.

In order to determine relative effective electrochemical surface area of M{Mo/W}S_x electrodes for the proton reduction reaction, these electrodes deposited on carbon glassy were first equilibrated in a pH 7 phosphate buffer solution by repeating 30 CVs from 0V to -0.20V *vs.* RHE with a potential scan rate of $50mV.s^{-1}$. Cyclic voltammograms were then recorded for these electrodes at -0.06V to +0.09V *vs.* RHE potential range with different potential scan rate (**figure S 12**). Absolute total current density i_a+i_c at 0V *vs.* RHE was plotted in function of potential scan rate (**figure S12**). Slope value of this plot is twice the double layer capacitance C_{dl} [*ref. 2*].

Effective electrochemical surface area can be deduced from C_{dl} and the area-averaged capacitance. The area-averaged capacitance value depends on electrode material. However, these values are not known for the M{Mo/W}S_x sulfides. We assume these sulfides have same area-averaged capacitance to estimate their relative effective electrochemical surface area (**table S1**).

Electrochemical impedance spectroscopy (EIS) analysis was conducted for MWS_x electrodes deposited on glassy carbon, with the same reference electrode, counter electrode and configuration previously stated. The measurements were performed with a potentiostat Autolab PGSTAT-30 equipped with a frequency analyser module. A small voltage perturbation (20 mV rms) was applied with frequencies ranging between 100 kHz and 0.1 Hz at different DC voltages in the region of interest. The results were fitted to the equivalent circuit in **figure S14** with a ZView software by Scribner Associated.

The morphologies of deposited films were investigated by Field Emission Scanning Electron Microscopy (FESEM, JEOL JSM-7600F) operated at 5 kV and Transmission Electron Spectroscopy (TEM, JEOL 2100F) operated at 200kV. For TEM analysis, the deposited materials were collected from FTO electrode, suspended into ethanol and drop casted on the lacey carbon copper grid.

The chemical composition was investigated by X-ray Photoelectron Spectroscopy (XPS) using an ultrahigh vacuum VG ESCALAB 220i-XL system equipped with a monochromatic Al *K*α (1486.6eV) source. The pressure in the analysis chamber was kept in the 10^{-10} Torr range. The hemispherical energy analyzer was calibrated with gold, silver and copper polycrystalline standard samples by setting the $Au4f_{7/2}$, $Ag3d_{5/2}$ and $Cu2p_{3/2}$ peaks at binding energies of 83.98±0.02, 368.26±0.02 and 932.67±0.02 eV. The survey and high-energy resolution scans were recorded with pass energies of 150 and 20eV, respectively. Quantitative analysis of the XPS spectra was carried out using a Shirley background subtraction before performing a least-square-error fit with a mixture of Gaussian and Lorentzian line shapes.

2. *In–situ* preparation of $[M(WS_4)_2]^{2-}$ complexes (M= Co, Ni) and electrodeposition of MWS_x thin films

$[M(WS_4)_2]^{2-}$ complexes (M= Co, Ni) were prepared *in-situ* in a pH 7 phosphate (KPi 0.1M) buffer solution. In 30mL oxygen-free KPi solution, 4.4mg $Co(NO_3)_2.6H_2O$ (15 µmol) and 10.5g $(NH_4)_2[WS_4]$ (30 µmol) were added resulting in a 0.5mM yellow solution of $[Co(WS_4)]^{2-}$. This solution remained stable under nitrogen for hours.

Similarly, an orange solution of 0.5mM $[Ni(WS_4)_2]^{2-}$ was prepared from $Ni(NO_3)_2.6H_2O$ and $(NH_4)_2[WS_4]$.

The UV-visible absorption spectrum of a 0.1mM $[Ni(WS_4)_2]^{2-}$ solution in comparison with that of a $(NH_4)_2[WS_4]$ (0.2 mM) solution is given in **figure S1**. New absorbance band peaking at 447nm was attributed to the electron transfer from the $[WS_4]^{2-}$ ligand to Ni^{2+} [*refs. 3,4*].

MWS_x thin films were deposited on carbon or FTO electrode from a 0.5 mM solution of $[M(WS_4)_2]^{2-}$ in pH 7 phosphate buffer either by repeating potential cycle (from 0V to –0.9V *vs.* Ag/AgCl) or by holding these electrodes at cathodic potential $E_{apl.}$ ($E_{apl.} \leq -0.3$ V for the Co case and $E_{apl.} \leq -0.4$V *vs.* Ag/AgCl for the Ni case). For the deposition on FTO electrode, the solution was magnetically stirred to limit mass-transport limitation. At applied potential of –0.62V *vs.* Ag/AgCl, the black grey thin film was visible after ca. 10 min deposition. Deposited MWS_x thin films were carefully washed with O_2-free deionised water then O_2-free ethanol. They were then kept under Ar atmosphere and at room temperature before transferred *ex-situ* to the spectrometer for analysis. Total air-exposed time during the sample transfer was ~3 min.

When carbon electrode was employed, it was slowly rotated at 100 rpm during deposition. All MWS_x/C electrodes employed for kinetic investigation were obtained by deposition at -0.70V *vs.* Ag/AgCl.

For comparison, $CoMoS_x$ film was deposited on C electrode (rotated at 100 rpm) at -0.55V *vs.* Ag/AgCl from a solution of 0.5mM $[Co(MoS_4)_2]^{2-}$ in pH 7 phosphate solution. This relative less negative constant potential was chosen to solely grow ternary $CoMoS_x$ phase. Indeed, no MoS_x (MoS_2 or MoS_3) deposition was evidenced at this potential employing a $[MoS_4]^{2-}$ solution free of Co^{2+} [*ref. 5*]

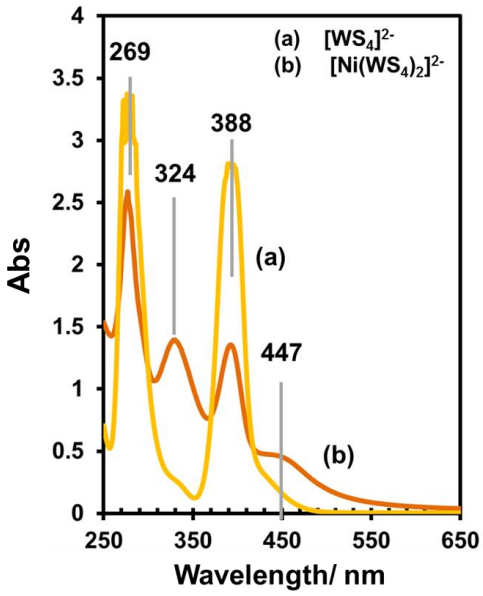

Figure S1: *Absorption spectra of $(NH_4)_2[WS_4]$ (0.2mM) and $[Ni(WS_4)]^{2-}$ (0.1mM) solution in pH 7 phosphate buffer (0.1M KPi).*

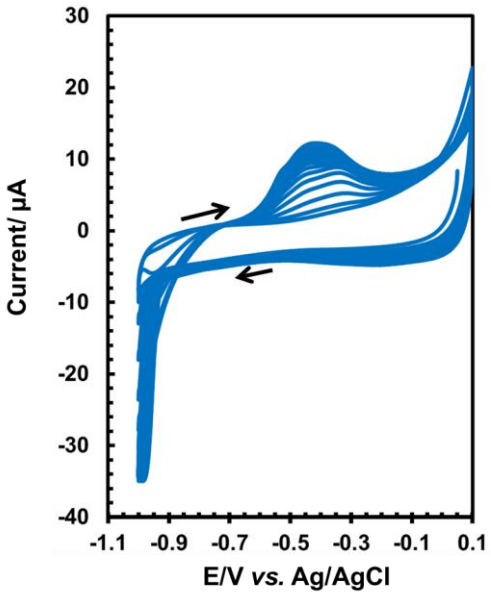

Figure S2: *Consecutive cyclic voltammograms of a 0.5mM $Co(NO_3)_2$ solution in pH 7 phosphate buffer (0.1M KPi) recorded on a glassy carbon electrode, potential scan rate of 50 $mV.s^{-1}$.*

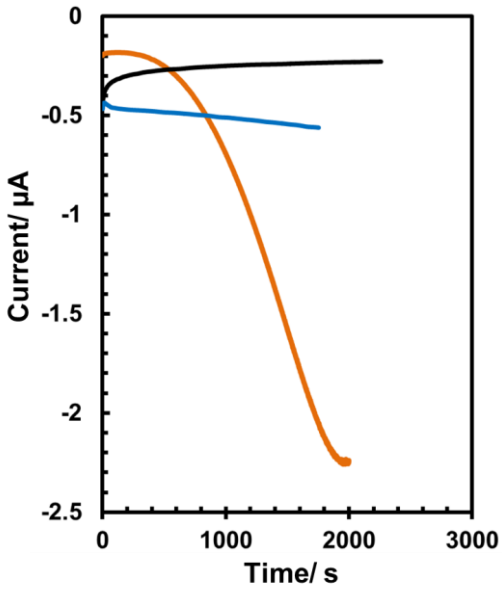

Figure S3: *I-t curves recorded on a carbon electrode (500 rpm) at –0.4V vs. Ag/AgCl for a solution of 0.5mM $[Ni(WS_4)_2]^{2-}$ (orange curve), 0.5mM $Ni(NO_3)_2$ (blue curve) or 1.0mM $(NH_4)_2[WS_4]$ (black curve) in pH 7 phosphate buffer (0.1M KPi)*

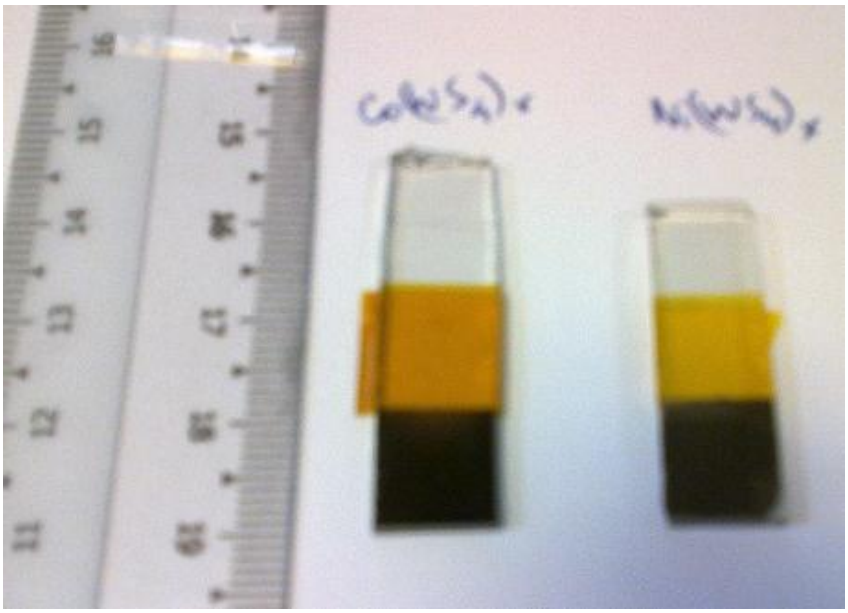

Figure S4*: Images of a $CoWS_x$ (left) and a $NiWS_x$ (right) thin film deposited on FTO electrode at –0.62V vs. Ag/AgCl for 1h*

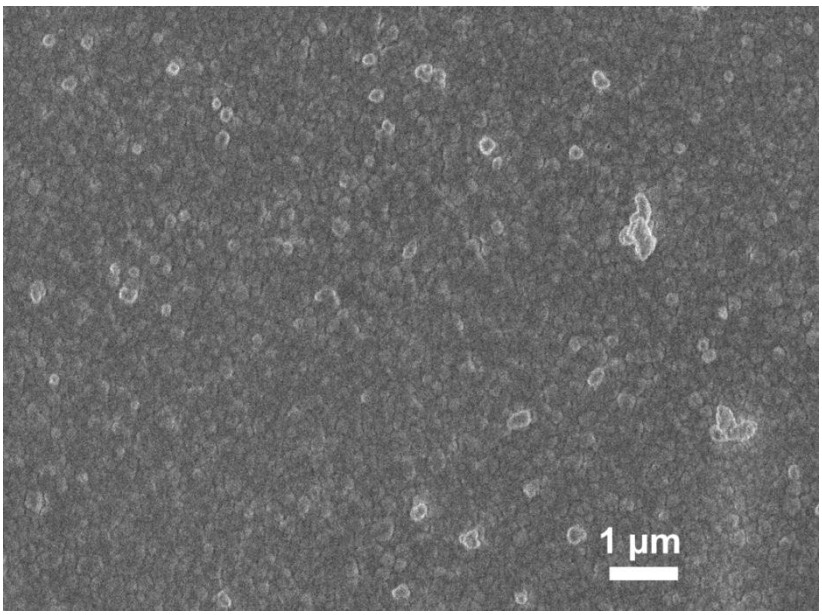

Figure S5: *SEM image collected on a $NiWS_x$ film deposited on FTO electrode at –0.62V vs. Ag/AgCl for 20 min (30 mC of charges were passed per 1cm^2 FTO).*

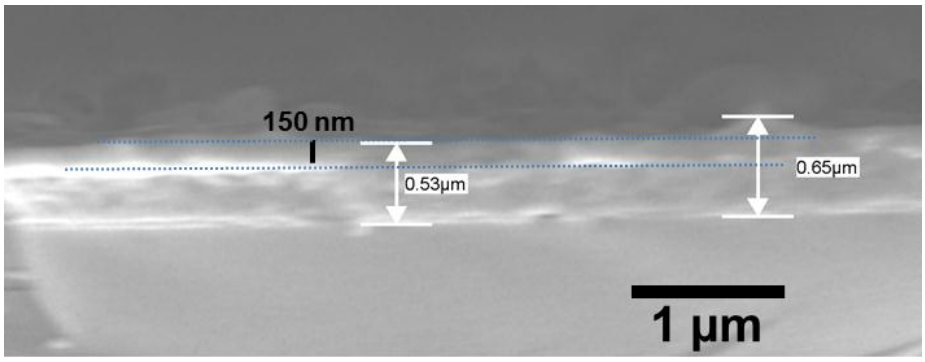

Figure S6: *Cross section image collected on a $NiWS_x$ film deposited on FTO electrode at –0.62V vs. Ag/AgCl for 1h. $NiWS_x$ film thickness was ca. 150 nm*

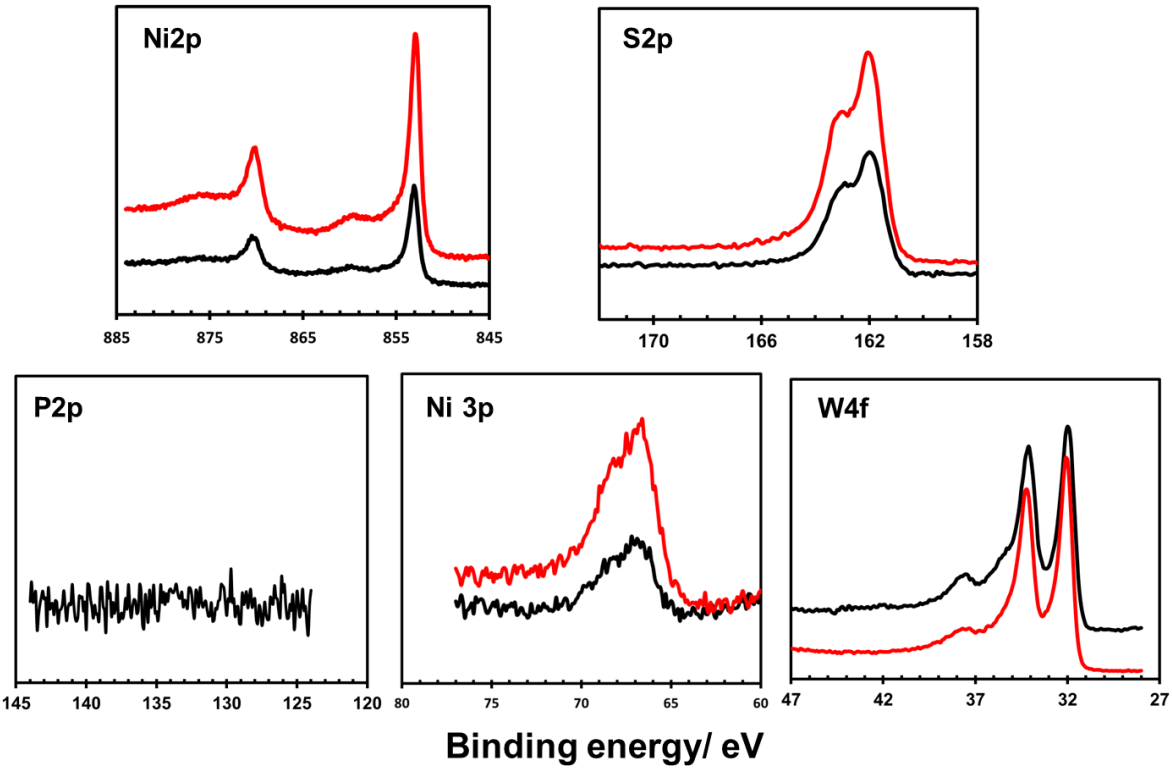

Figure S7: *XPS analysis on $NiWS_x$ deposited at –0.62V (red curves) and –1.0V vs. Ag/AgCl (black curves) on FTO electrode employing 0.5mM $[Ni(WS_4)_2]^{2-}$ solution in pH 7 phosphate buffer (0.1M KPi). $Ni2p_{3/2}$ peak was observed at 853.2 eV. $W4f_{7/2}$ was found at binding energy*

of 32.1eV while two peaks were found at 162.7 and 161.6eV for the S2p$_{3/2}$. These binding energies are similar to those reported for a NiWS single phase [ref. 6]. P was not found in the deposited NiWS$_x$ film.

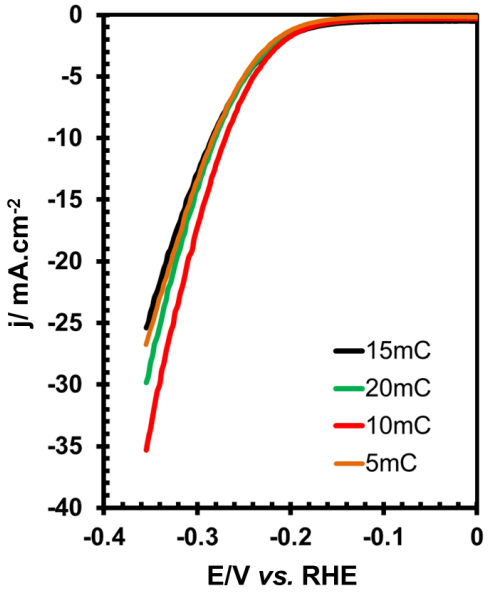

***Figure S8**: I-V curves recorded in a pH 7 phosphate solution for X mC CoWS$_x$ electrodes deposited on carbon glassy electrode at constant potential of -0.7 V vs. Ag/AgCl by passing X mC of charges for deposition. Potential scan rate was 2mV.s^{-1}. Electrode was rotated at 1000 rpm.*

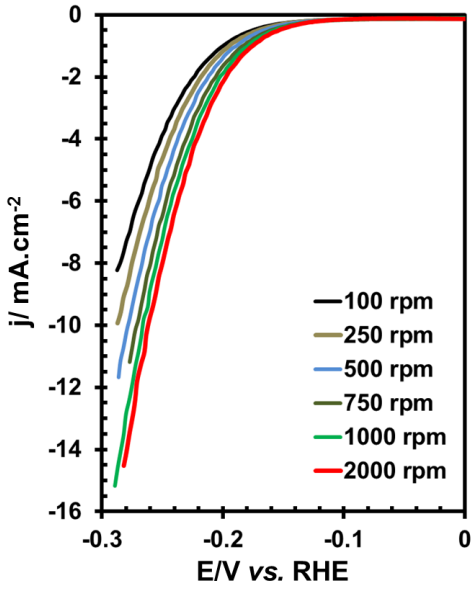

***Figure S9**: I-V curves recorded for a 10mC $CoWS_x$ electrode in pH 7 phosphate buffer solution at different electrode rotating rate.*

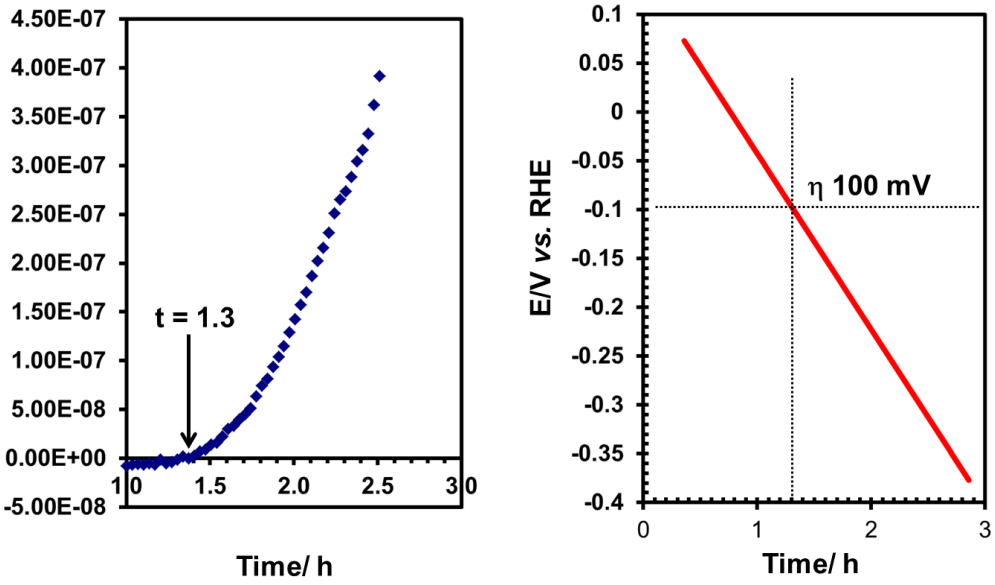

Figure S10: *Left: H_2 production analysis by a GC coupled to a $CoWS_x$/FTO catalyst electrode under a cathodic potential polarization (potential scan rate of 0.05mV.s^{-1}). Right: E-t curve recorded on this $CoWS_x$ electrode.*

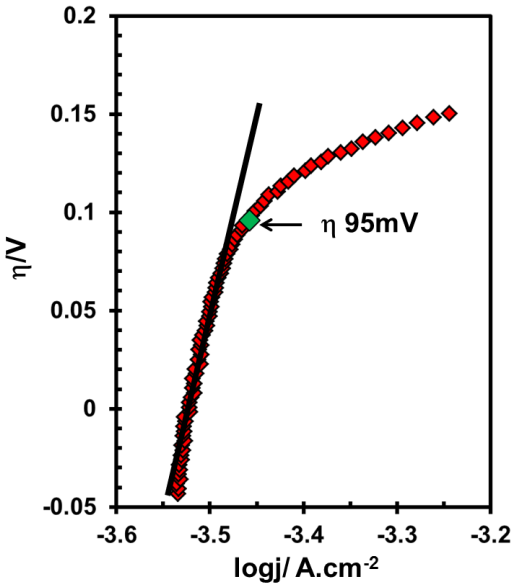

Figure S11: *Tafel plot (in low current density region) for a $CoWS_x$ catalyst film in a pH 7 phosphate buffer solution. Potential scan rate was of 2mV.s^{-1}. Electrode was rotated at 1000 rpm.*

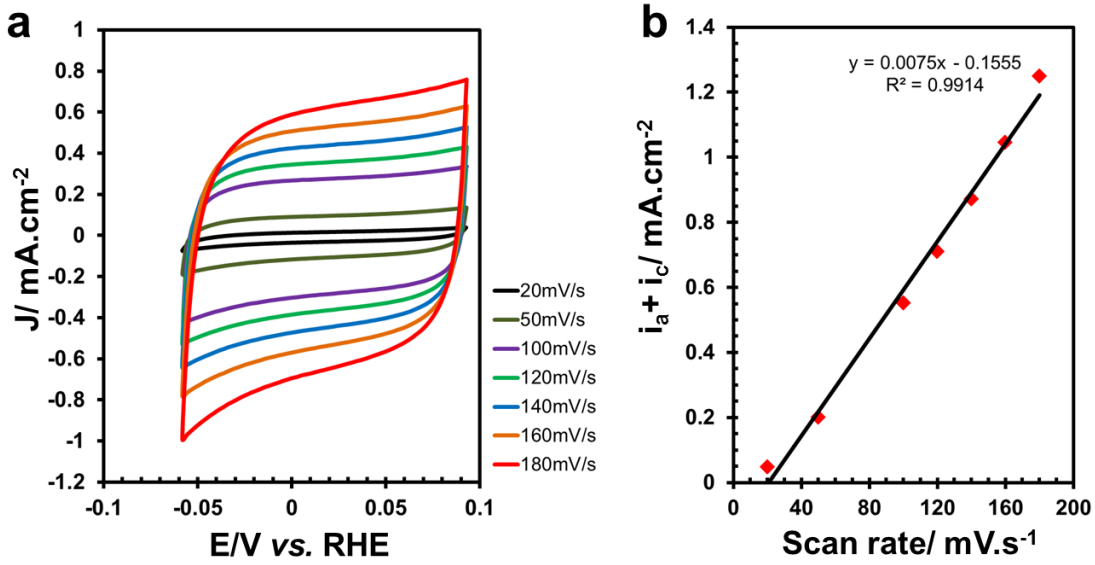

***Figure S12**: (**a**) Cyclic voltammograms recorded at different scan rates in a phosphate solution buffered at pH 7 for a 10mC $CoWS_x$ electrode deposited on carbon electrode. (**b**) Evolution of charging current at 0V vs. RHE as a function of potential scan rate*

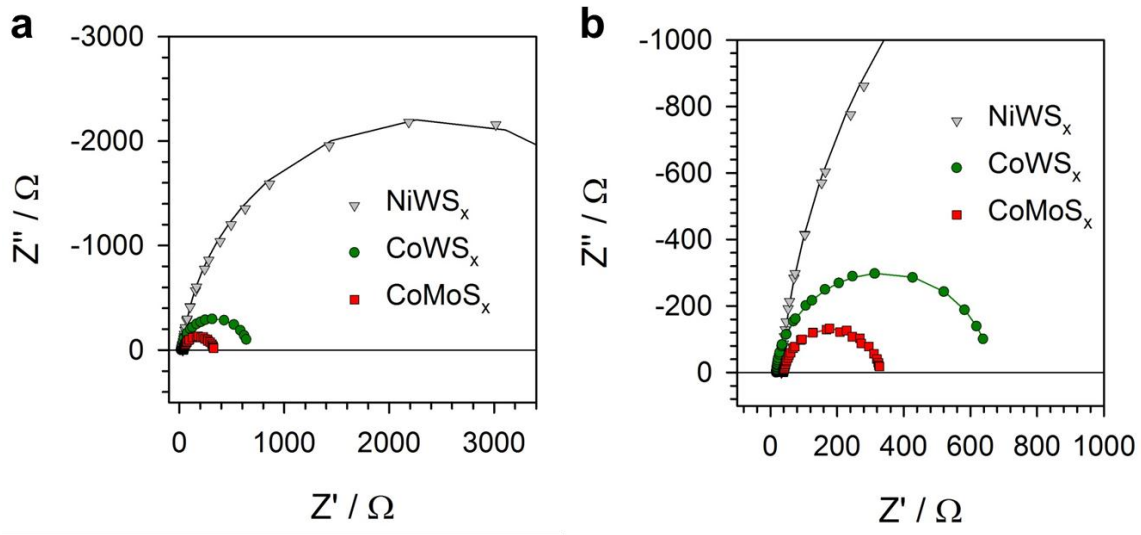

***Figure S13**: Example of Nyquist plots showing EIS responses of ternary metal sulfide electrodes at -0.2V vs. RHE at pH 7 phosphate buffered solution.*

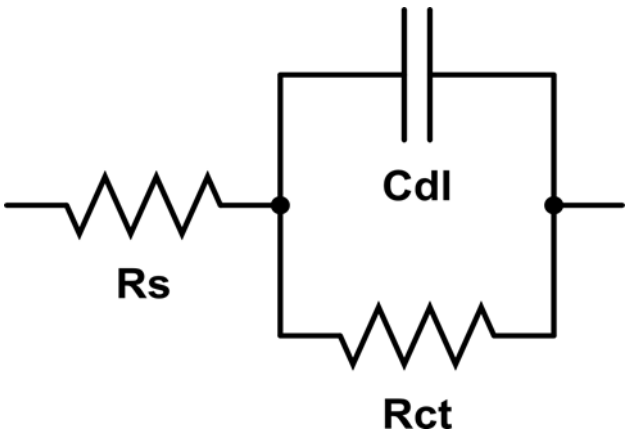

Figure S14: *Equivalent circuit employed to fit the EIS results.*

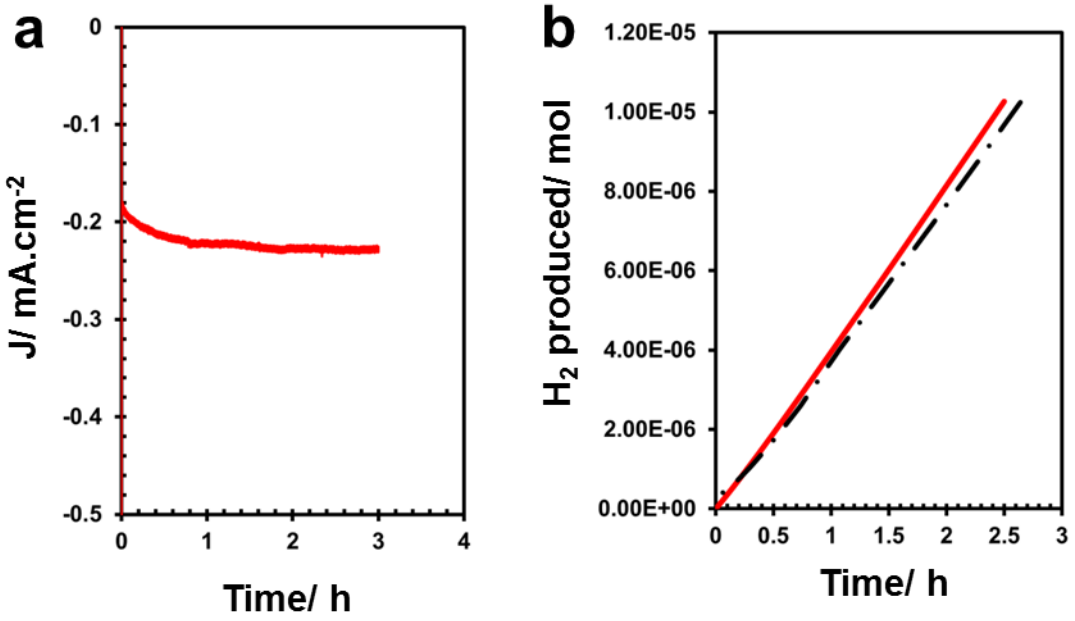

***Figure S15**: Bulk electrolysis at η 0.275V employing a $NiWS_x$ electrode: I-t curve (a); theoretical (bulk red curve) and actual (black trace curve) for H_2 production as a function of electrolysis time (b)*

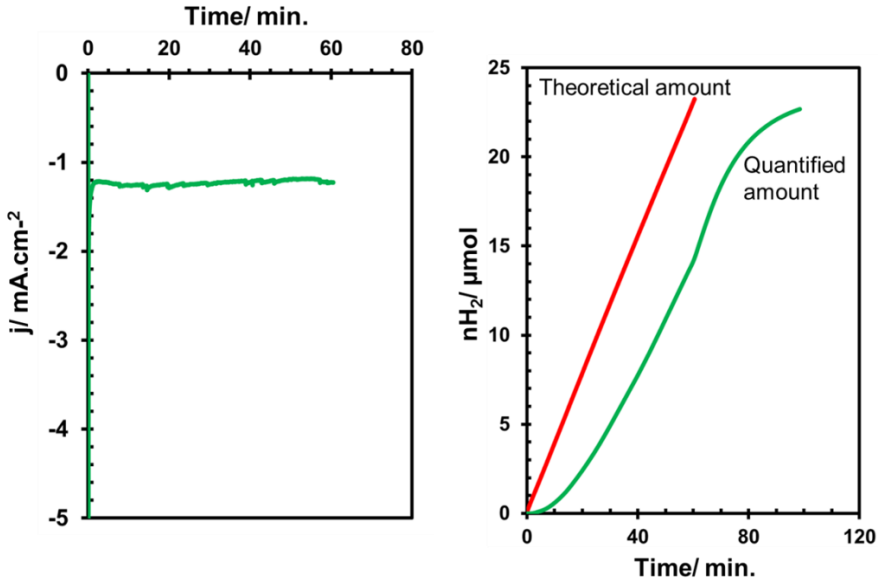

Figure S16: *Bulk electrolysis at –0.375V vs. RHE in a pH 7 phosphate buffer (0.1M KPi) using a $CoWS_x$ electrode deposited on FTO (1cm^2). I-t curve is given (left). Hydrogen release quantified by GC during bulk electrolysis compared with to hydrogen production theoretically calculated based on the Nernst equation (right).*

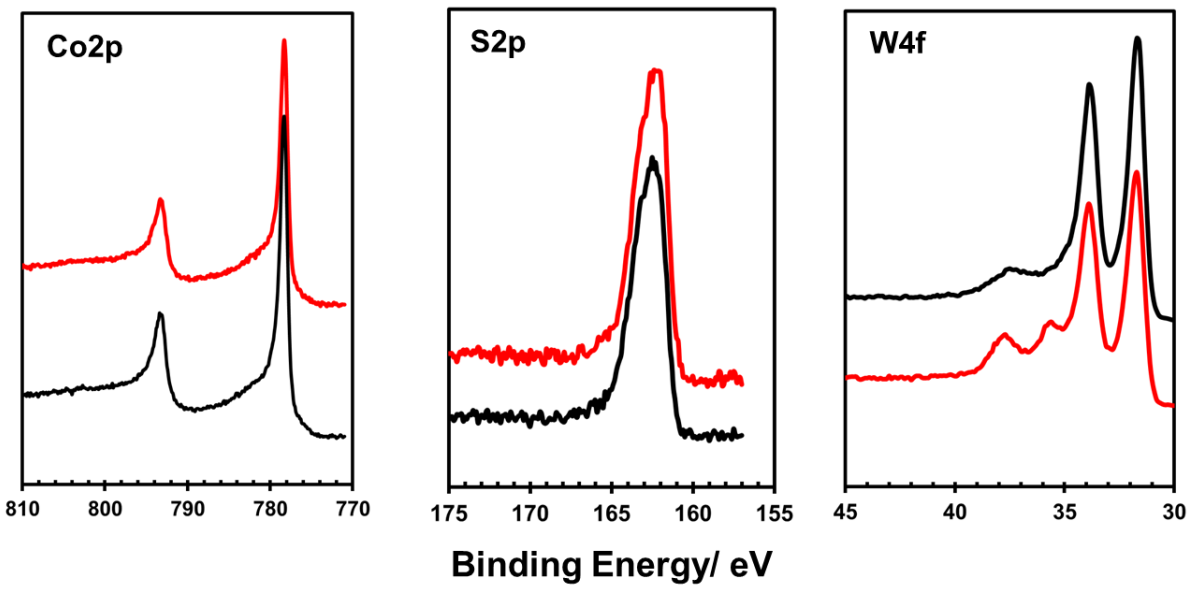

Figure S17: *XPS analysis on an as-deposited $CoWS_x$ catalyst film (black curves) and after extended catalytic condition at –0.375V vs. RHE for 2h (red curves)*

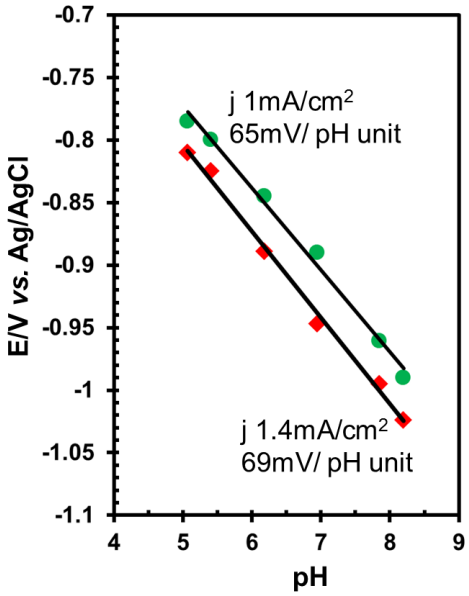

Figure S18: *Potential E_j required to be applied on a $NiWS_x$ electrode as a function of pH to sustain a catalytic current j.*

Table S1: *Double layer capacitance and relative electrochemical surface area of 10mC M{Mo/W}S_x electrodes*

	$NiWS_x$	***$CoWS_x$***	***$CoMoS_x$***
Current *vs.* scan rate slop	*0.002*	*0.0075*	*0.0108*
Relative C_{dl}	*1.0*	*3.75*	*5.40*
Relative electrochemical surface area	*1.0*	*3.75*	*5.40*

References

1 Cobo, S. *et al.* A Janus cobalt-based catalytic material for electro-splitting of water. *Nature Materials* **11**, 802-807 (2012).

2 Bard, A. J. & Faulkner, L. R. Electrochemical methods: Fundamentals and Application. *John Willey and Sons, INC.* **Second Edition** (2001).

3 Müller, A., Diemann, E., Jostes, R. & Bögge, H. Transition Metal Thiometalates: Properties and Significance in Complex and Bioinorganic Chemistry. *Angewandte Chemie International Edition in English* **20**, 934-955, doi:10.1002/anie.198109341 (1981).

4 Callahan, K. P. & Piliero, P. A. Complexes of d8 metals with tetrathiomolybdate and tetrathiotungstate ions. Synthesis, spectroscopy, and electrochemistry. *Inorganic Chemistry* **19**, 2619-2626, doi:10.1021/ic50211a029 (1980).

5 Tran, P. D. & et al. Unpublised data.

6 Coulier, L., Kishan, G., van Veen, J. A. R. & Niemantsverdriet, J. W. Influence of Support-Interaction on the Sulfidation Behavior and Hydrodesulfurization Activity of Al2O3-Supported W, CoW, and NiW Model Catalysts. *The Journal of Physical Chemistry B* **106**, 5897-5906, doi:10.1021/jp0136821 (2002).